https://doi.org/10.1016/j.electacta.2017.05.182

A micro membrane-less photoelectrochemical cell for hydrogen and electricity generation in the presence of methanol

Zhibin Wang[a,b], Yingying Lin[a,b], Rong Chen[a,b*], Qiang Liao[a,b], Xun Zhu[a,b*], Liang An[c*], Xuefeng He[a,b], Wei Zhang[a,b]

[a] Key Laboratory of Low-grade Energy Utilization Technologies and Systems (Chongqing University), Ministry of Education, Chongqing 400030,China

[b] Institute of Engineering Thermophysics, Chongqing University, Chongqing 400030, China

[c] Department of Mechanical Engineering, The Hong Kong Polytechnic University, Hong Kong, China

[a,b] Tel.: 0086-23-65103119; fax: 0086-23-65102474; e-mail: rchen@cqu.edu.cn (Rong Chen)

[a,b] Tel.: 0086-23-65102474; fax: 0086-23-65102474; e-mail: zhuxun@cqu.edu.cn (Xun Zhu)

[c] Tel.: 852-27667820; fax: 852-23654703; e-mail: liang.an@polyu.edu.hk (Liang An)

Abstract

In present study, a micro membrane-less photoelectrochemical cell (μML-PEC) is developed for simultaneous hydrogen and electricity productions in the presence of methanol, in which the photoanode of a TiO_2 film is consisted of a compact layer at the bottom and a porous layer on the top. The experimental results indicate the PEC miniaturization, and the membrane elimination, and the addition of a compact layer can enhance the mass, electron and photon transfer, which eventually boosts the performance. The performance of the developed μML-PEC is also evaluated under various operating conditions, including the light intensity, methanol and electrolyte concentrations and flow rate. It is shown that the maximum power density increases and the fill factor (FF) and solar-to-hydrogen conversion efficiency (STH) decrease with increasing the light intensity. For the electrolyte concentration, the maximum power density and STH and FF all increases with increasing the electrolyte concentration. Once the electrolyte is high enough, its effect become insignificant. Besides, the increase of the methanol concentration and the decrease of the flow rate

are beneficial for the improvement in the performance. The obtained results reveal that the μML-PEC developed in this work shows the promising potential for simultaneously producing electricity and hydrogen in the presence of methanol.

Keywords: PEC; Hydrogen production; Electricity production; Fill factor; STH

1. Introduction

Presently, the environmental problem has become one of the grand challenges all over the world [1]. In particular, a large amount of wastewater is discharged into natural water body every year, which threatens the ecological system and human health. Hence, extensive methods have been proposed to address the water pollution problem. Since the photoelectrochemical water splitting using titanium dioxide (TiO_2) was successfully reported by Fujishima and Honda [2], both the photocatalytic [3-7] and photoelectrochemical [8-10] technologies have been widely applied into wastewater treatment [11-12], organic pollutants mineralization [13], water and air disinfection [14], CO_2 photoreduction [15-17] and electricity production [18-20] and so on. Among them, the photoelectrochemical cell that can degrade organic substances to generate hydrogen or electricity is a promising technology for simultaneous wastewater treatment and renewable energy supply [21]. Hence, the photoelectrochemical cell has received ever-increasing attention toward the sustainable environmental and energy development.

In the past, numerous efforts have been devoted to the development of the photoelectrochemical cell. Antoniadou *et al.* [22] developed undoped and Ru-doped commercial nanocrystalline TiO_2 anatase as photocatalyst to produce hydrogen and electricity. They used quantum dot sensitized nanocrystalline titania photoanodes to construct the photoelectrochemical cell for producing electricity or hydrogen [23]. Daskalaki *et al.* [24] studied the photoelectrochemical degradation of waste material in aqueous solutions and hydrogen production using both powdered and immobilized Pt/CdS/TiO_2 photocatalysts as the photoanode. Zhang *et al*. [25] prepared Au nanoparticles sensitized ZnO nanorod@nanoplatelet (NR@NP) core–shell arrays for

the photoelectrochemical cell. The results showed that Au–ZnO NR@NP nanoarray exhibited enhanced photocurrent density and incident-photon-to-current-conversion efficiency.

It can be found that existing works are mainly focused on the photocatalysts development and the photoanode microstructure. In fact, the design of the photoelectrochemical cell is also of importance for improving the performance because it affects the mass and photon transport. Previous photoelectrochemical cells usually employed the two-compartment structure with the photoanode and cathode separated by an ion-transport membrane. For instance, Antoniadou *et al.* [26-27] presented an H-shaped photo-fuel cell to produce electricity, in which the cell consisted of a TiO_2-coated photoanode, a cathode and a proton exchange membrane. Hernández-Pagán *et al*. [28] built a two-compartment four-electrode H-shaped PEC for water splitting. Tang *et al.* [29] proposed an aqueous-film rotating disk photocatalytic fuel cell (RDPFC) for the simultaneous hydrogen and electricity production along with the degradation of dye wastewater. Yang *et al*. [30] presented a dual rotating disk photocatalytic fuel cell for wastewater treatment, which was consisted of a rotating photoanode, a rotating cathode and a proton exchange membrane. However, in these designs, not only the size of the PEC but also the distance between the two electrodes is large, which increases the mass and ion transfer resistances. Meanwhile, the ion-transport membrane also increases the capital cost of the PEC. It is well known that the miniaturization of the reactors can dramatically enhance the mass transport as a result of large surface-to-volume ratio. In this study, therefore, to address the above-mentioned issues encountered in conventional PECs, a micro membrane-less photoelectrochemical cell (μML-PEC)

was developed for simultaneous hydrogen and electricity productions in the presence of methanol. The developed μML-PEC was consisted of a TiO_2 photoanode, a Pt/carbon paper cathode and a reaction microchamber without the membrane. The methanol and electrolyte mixture in the cell was maintained to be laminar flow. The performance of the developed μML-PEC was then evaluated by studying the effects of the light intensity, the concentrations of the methanol and electrolyte, and the liquid flow rate under the alkaline condition. The fill factor and solar-to-hydrogen conversion efficiency were also calculated.

2. Experimental

2.1 Structure of μML-PEC

The developed μML-PEC was consisted of a photoanode, a reaction microchamber, a cathode and cathode cover plate, which were stacked in a sandwiched structure. The cathodic electrode was sealed by the cathode cover plate to avoid the oxygen reduction reaction and to ensure the hydrogen production at the cathode. Fig. 1a shows the schematic of the developed μML-PEC. As shown, the reaction microchamber was consisted of a triangular inlet and a triangular outlet and a rectangular microchamber in the middle. The purpose of the triangular design was to ensure the uniform filling to the reaction microchamber. The size of the rectangular microchamber was 1.5×3.0 cm, and the depth corresponding to the distance between the electrodes was 1000 μm. The photoanode was manufactured by coating TiO_2 on the FTO conducting glass. The cathode was made of a Pt-black deposited carbon paper. Each electrode had an active area of $1.0\times1.0=1.0$ cm^2, which was located in the center of the microchamber. Two holes were drilled in the FTO conducting glass

functioning as the inlet and outlet, respectively. The image of the fabricated μML-PEC is shown in Fig. 1b.

2.2 Photoanode preparation

As mentioned above, the photoanode was prepared by coating TiO_2 on the FTO conducting glass (resistance 8 Ω per square, Xinyan Technology Co., China) to form a TiO_2 film. In this work, the TiO_2 film consisted of two layers of a bottom compact layer and a top porous layer. The bottom compact layer could ensure the strong adhesion of the TiO_2 film to the FTO conducting glass [19] and provide high conductivity to prevent the recombination of photo-excited electro-hole pairs [31], while the top porous layer could provide sufficient path for the mass and photon transport and large specific surface area for the photoelectrochemical reactions [32]. The bottom compact layer was prepared by the spin-coating method using densely packed TiO_2 layer solution (Kunshan Sunlaite New Energy technology Co., China). The top porous TiO_2 layer was fabricated by the wet spray method [18]. Prior to the fabrication of the TiO_2 film, the FTO conducting glass was firstly cleaned by sonication in acetone, isopropanol and ethanol. Densely packed TiO_2 layer solution was then spin-coated on the FTO conducting glass. After that, it was calcined at 500°C for 30 minutes to form a compact TiO_2 layer. On the top of this compact layer, a porous TiO_2 layer was fabricated by the wet spray method. First, 12 g TiO_2 nanoparticles (Aeroxide P25, Acros, Belgium) were dispersed in a mixture of 120 mL DI water and 0.4 mL acetylacetone (Sigma-Aldrich, USA) with magnetic stirring. Then 0.2 mL of a Triton X-100 (Sigma-Aldrich, USA) was added to facilitate the spreading of the colloid. Afterwards, 2.4 g polyethylene glycol (Aladdin, China) was added into the solution. The solution was then mixed for 12 hours to form the TiO_2

colloid. The prepared colloid was sprayed onto the compact layer by a spray gun and finally calcined at 550 °C for 2 hours to form the porous TiO_2 layer. Total TiO_2 loading was about 3.0 mg cm^{-2}.

2.3 Cathode preparation

The cathode was made by depositing Pt-black on carbon paper. Here, the hydrophobic carbon paper with the coated carbon powders (HCP120, Hesen, China) was used as received. The catalytic layer was prepared by the following steps. 0.1 g Pt-black (CX0375, Alfa Aesar, USA) was firstly mixed with 0.5 g Nafion perfluorinated resin (D520, 5% wt. solution in lower aliphatic alcohols and water, Du Pont Co., USA) and 5 g solution containing 2.5 g ethanol and 2.5 g deionized water. After ultrasonic agitation for 30 min, the mixture was sprayed onto the carbon paper and then heated at 80 °C for 30 min. The Pt-black loading was about 1.0 mg cm^{-2}.

2.4 Experimental setup and instrumentations

In this experiment, the prepared photoanode samples were characterized by an X-ray diffractometer (XRD, Max-2600, Rigaku D, Japan) and the scanning electron microscope (SEM, S-4800, Hitachi, Japan). KOH was chosen as the electrolyte, which was dissolved in water to form the electrolyte solution. After that, methanol was added into the KOH aqueous solution to form the KOH and methanol mixture. The prepared solution was introduced into the developed μML-PEC by a syringe pump (BT100, Longer Pump, China). A LED UV lamp with the wavelength of 370 nm was used. The light intensity was controlled by adjusting the distance between the μML-PEC and the lamp and measured by an UV-radiometer (FZ-A, Photoelectric

Instrument Factory of Beijing Normal University, China). The polarization curve was recorded by an electrochemical workstation (Zennium, Zahner, Germany). The hydrogen gas was detected by a gas chromatograph (Trace 1300, Thermo Scientific, USA).

3. Results and discussion

3.1 Working principle of μML-PEC

During the working process, the electrolyte with methanol is continuously supplied into the reaction microchamber. Upon illumination, the TiO_2 photoanode is photo-irradiated to produce electron-hole pairs,

$$TiO_2 + h\nu \rightarrow TiO_2\ (e^- + h^+) \quad (1)$$

Typically, the photo-generated holes are more likely to be scavenged by OH^- ions in the alkaline environment to form hydroxyl radicals that have strong oxidation ability,

$$OH^- + h^+ \rightarrow OH^\cdot \quad (2)$$

Methanol can then be oxidized by hydroxyl radicals to generate water and methoxy radical,

$$CH_3OH + OH^\cdot \rightarrow H_2O + CH_2OH^\cdot \quad (3)$$

The redox potential of methoxy radical allows it to inject an electron into the energy conduction band of the TiO_2, while formaldehyde is generated [33],

$$CH_2OH^\cdot + OH^- \rightarrow H_2O + CHOH + e^- \quad (4)$$

This extra electron injection is typically referred to as the current doubling effect in the presence of organics [33-34]. Since formaldehyde is easily to be oxidized to

formic acid, it is photo-oxidized via the following mechanism,

$$CHOH + 2OH^- + h^+ \rightarrow HCOOH + H_2O + e^- \quad (5a)$$

or

$$CHOH + OH\cdot + OH^- \rightarrow HCOOH + H_2O + e^- \quad (5b)$$

The generated formic acid reacts with OH^- in the alkaline environment,

$$HCOOH + OH^- \rightarrow COOH^- + H_2O \quad (6)$$

The formic ion can be directly oxidized to carbon dioxide by photo-generated holes due to the strong adsorption to TiO_2 [35-36],

$$COOH^- + h^+ + OH^- \rightarrow + H_2O + CO_2 + e^- \quad (7)$$

The generated electrons go through the external load to the cathode, where water and electrons are then reduced to hydrogen and OH^- ions in the absence of oxygen under the alkaline condition [23, 37, 38],

$$2H_2O + 2e^- \rightarrow H_2 + 2OH^- \quad (8)$$

The generated OH^- ions are directly transferred to the photoanode in the solution, completing the circuit.

3.2 XRD and SEM characterization of the photoanode

XRD patterns of the TiO_2 samples were characterized by an X-ray diffractometer and the results are shown in Fig. 2a. The crystalline diffraction peaks of the TiO_2 layer at 2θ of 25.3°, 37.9°, 38.6°, 48.1°, 53.9°, 55.2° and 62.7° were identified as the anatase-TiO_2. The rutile phases were also observed at 2θ of 27.4°, 36.1° and 41.3° with comparatively weak intensity. Because the TiO_2 film was coated on the FTO

conducting glass, the cassiterite-SnO_2 phases were also observed. The morphology of the prepared TiO_2 film on the FTO conducting glass was characterized by the SEM. From the top view shown in Fig. 2b, it can be found that the TiO_2 nanoparticles were uniformly distributed on the FTO conducting glass. Numerous micro pores were formed. This porous structure not only provides large specific surface area for the photoelectrochemical reactions but also offers plenty of path way for the mass and photon transport. Fig. 2c displays the cross-section view of the prepared photoanode. The porous structure of the TiO_2 film at the cross section was similar to the one obtained from the top view. The thickness of this layer was about 30 μm. Because the compact layer was rather thin, only the porous layer could be observed in this resolution. To more clearly show the compact TiO_2 layer, the high-resolution SEM characterization was also performed, as shown in Fig. 2d. A rather dense TiO_2 layer was observed, whose thickness was about 120 nm.

3.3 Performance evaluation of μML-PEC

In this section, the performance of the μML-PEC was evaluated, including the photo-response behavior, the polarization curve and the long-term operation. In this testing, the light intensity was 5 mW cm^{-2}, methanol and KOH concentrations were 0.5 M and 0.2 M, and the flow rate was kept at 100 μL min^{-1}.

3.2.1 Photo-response behavior

To characterize the photo-response behavior of the developed μML-PEC, two feature

parameters of the short circuit current density and open circuit voltage (OCV) were chosen to study the photo-response behavior. Fig. 3a shows the photo-response of the OCV to the light on/off mode. It can be seen that when the light was on, the cell voltage instantly climbed to about 0.92 V. When the light was off, the cell voltage quickly dropped. In the light-off period of 300 s, the cell voltage dropped to about 0.16 V. The photo-response behavior of the short circuit current density under the light on/off mode is shown in Fig. 3b. It can be seen that once the illumination was applied, the photocurrent density immediately shifted from 0 to about 1 mA cm^{-2} and then gradually increased to 1.13 mA cm^{-2}. When the light was off, the photocurrent was immediately restored to almost zero. Such behaviors were well reproduced during several on/off testing cycles. These results indicate that the developed μML-PEC shows a good photo-response to the illumination.

3.2.2 The typical polarization curve

The polarization curve was measured at a scan rate of 2 mV s^{-1} by an electrochemical workstation. The typical polarization curve of this μML-PEC is shown in Fig. 4a. It can be seen that the OCV was about 0.92 V. With increasing the current density, the cell voltage was reduced as a result of the increased overpotentials of both the photoanode and cathode associated with the photoelectochemical and electrochemical kinetic losses and ohmic loss. When the cell voltage was below about 0.35 V, both the current density showed the almost unchanged trend, that is, the cell voltage sharply reduced at high current densities. In traditional fuel cells, this phenomenon is typically

attributed to the concentration polarization, namely the mass transfer loss, on the account of the limited reactant supply. For the μML-PEC, the low cell voltage indicates that the potential difference between the photoanode and cathode is small. In this case, the driving force for the transfer of photo-excited electrons to the cathode was weakened. The electrons and holes were then easily recombined. The reduced amount of holes led to less hydroxyl radical to be generated. As a consequence, the lowered hydroxyl radical concentration greatly slowed down the photoelectrochemical reaction rate, which caused the cell voltage to be rapidly decreased. Therefore, the cell voltage was sharply decreased at high current densities.

With the polarization curve, two parameters can be determined to characterize the performance. One is the fill factor (FF), which is the ratio of the achieved maximum power density $(JV)_{max}$ to the theoretical maximum power density determined by the short circuit current density (J_{sc}) multiplying the OCV (V_{oc}),

$$FF = (JV)_{max} / J_{sc} V_{oc} \quad (9)$$

With Eq. (9), the fill factor of this μML-PEC under given operating conditions could be determined to be 0.42. The second parameter is to calculate the solar-to-hydrogen (STH) conversion efficiency, which has been widely used to characterize the performance of the photoeletrochemical cell without considering the faradic efficiency of the H_2 production [39-42]. Therefore, the STH of the developed μML-PEC can be determined by the following equation,

$$STH = \frac{1.23 J_{sc}}{P_{in}} \quad (10)$$

where P_{in} is the power of incident light. In this work, STH represents the ratio of the produced hydrogen energy to the incident light energy.

For given conditions, the STH of this μML-PEC operating with 0.5-M methanol could reach 30.5%. We also compared the STH obtained in present study with previous works, as listed in Table 1. It can be seen that the STH of the μML-PEC operating with 0.5-M methanol was higher than other previous works. This may be due to the fact that the mass and photon transfer was enhanced by the microreactor design and the addition of the compact layer into the photoanode enhanced the electron transport.

3.2.3 Long-term performance

The long-term performance is an important factor describing the PEC operation stability in practical applications. In order to study the operation stability of the developed μML-PEC, the long-term performance was measured at a constant discharging current density of 0.2 mA cm^{-2} for 10 hours. The result is presented in Fig. 4b. As shown, the cell voltage of the developed μML-PEC was rather stable. During the 10-hour continuous operation, the cell voltage just slightly declined from about 0.72 V to 0.70 V. It is revealed that the μML-PEC developed in this work can yield a relatively stable performance for future applications. Besides, the gaseous phase evolution from the Pt-black cathode can be found in this process. The gaseous phase was collected and detected using gas chromatography. It was proved that the gaseous phase contained hydrogen gas. This result implies that the developed μML-PEC can

be used to generate hydrogen in the presence of methanol under the alkaline condition.

3.4 Effect of light intensity

In PECs, the photoanodic reactions are actuated by the incident light. Therefore, the light intensity is one of the most important parameters affecting the performance. To study the effect of the light intensity, the methanol and electrolyte concentrations were kept at 0.5 M and 0.2 M, respectively, and the flow rate was kept at 100 μL min^{-1}, and the light intensity varied from 3 to 10 mW cm^{-2}. The results are shown in Fig. 5. It can be found from this figure that as the light intensity increased, the performance of the μML-PEC was improved, including the OCV and short circuit current density. It is easy to understand that the stronger the light intensity, the more photo-generated electron/hole pairs. As a result, the photoelectrochemical reaction rate at the photoanode was greatly enhanced, leading to the increased performance. Correspondingly, the maximum power density was increased with increasing the light intensity. As shown in Fig. 5b, the maximum power density was increased from 0.28 mW cm^{-2} to 0.91 mW cm^{-2} with increasing the light intensity. However, it was found that the STH and FF of the developed μML-PEC were reduced with increasing the light intensity. The STH was reduced from 30.7% to 28.7% and the FF was reduced from 0.44 to 0.40. The reduction of the STH could be attributed to the increased probability of the electron/hole recombination at high light intensities [18], which thereby lowered the solar energy utilization efficiency, although more electron/hole

pairs could be generated. For the FF, although the maximum power density was increased with the light intensity, the increase of the OCV and short circuit current density was more significant, thereby leading to the reduction of the FF with increasing the light intensity.

3.5 Effect of methanol concentration

In this study, the developed μML-PEC is used to produce electricity and hydrogen in the presence of methanol so that the methanol concentration has a significant influence on the performance. To study the effect of methanol concentration, the light intensity was maintained at 5 mW cm^{-2}, and the electrolyte concentration and flow rate were kept at 0.2 M and 100 μL min^{-1}, respectively. The methanol concentration ranged from 0.01 to 1.0 M. The results are given in Fig. 6. It can be seen that the performance was greatly affected by the methanol concentration. As shown, when the methanol concentration increased from 0.01 to 0.5 M, the J_{sc} was rapidly increased. When the methanol concentration was further increased to 1.0 M, the difference between 0.5 M and 1.0 M was almost neglected. When the methanol concentration was as low as 0.01 M, the change trend of the polarization curve was different with the cases with high methanol concentrations. At low current density region (< 0.1 mA cm^{-2}), the cell voltage showed a quick reduction with increasing the current density. This is because that the photoanode performance was mainly dependent on the kinetics at the photoanode at low current densities. The activation loss with the critically low methanol concentration is much larger than the cases with high

methanol concentrations, leading to a quick reduction in the cell voltage. In the meantime, because of the mass transfer limitation, the short circuit current density was much small. When the methanol concentration was increased to 0.5 M, the problem of the mass transfer limitation became weak, resulting in the improved cell performance at moderate and high current densities. The significant improvement in the cell performance can be attributed to increased current doubling effect due to the enhanced methanol transport. Therefore, the J_{sc} was rapidly increased when the methanol concentration was increased from 0.01 M to 0.5 M. As shown in Fig. 6a, the short circuit current density was increased from 0.72 mA cm^{-2} to 1.24 mA cm^{-2} as the methanol concentration was increased from 0.01 M to 0.5 M. However, the OCV was higher than those operating with relatively higher methanol concentrations, indicating that the effect of the methanol oxidation at the cathode was insignificant at extremely low methanol concentration. When further increasing the methanol concentration to 1.0 M, the mass transfer problem disappeared. Therefore, almost no increment of the short circuit current density was observed. Similarly, as shown in Fig. 6b, the maximum power density and STH were rapidly increased from 0.28 mW cm^{-2} to 0.48 mW cm^{-2} and from 17.7% to 30.4%, respectively, as the methanol concentration was increased to 0.01 M and 0.5 M. For the fill factor, it was quickly increased from 0.39 to 0.42 when the methanol concentration increased from 0.01 to 0.1 M, and gradually increased to 0.43 as the methanol concentration was further increased to 1.0 M. The increasing of FF is due to the reduction of the OCV with increasing the methanol concentration.

3.6 Effect of electrolyte concentration and flow rate

In this section, the effects of the electrolyte concentration and the flow rate on the performance were studied. To do this, the methanol concentration and the light intensity were kept at 0.5 M and 5 mW cm^{-2}, respectively. Fig. 7 shows the effect of the electrolyte concentration. Here, the flow rate was kept at 100 μL min^{-1}. As shown, the V_{oc} was the almost same in all cases, and the J_{sc} was increased with increasing the electrolyte concentration. The reason is that increasing the concentration of electrolyte is able to scavenge more photo-excited holes to generate more hydroxyl radical, which then enhances the photoelectrochemical reaction at the photoanode. Meanwhile, the increased electrolyte concentration also enhanced the electrochemical reaction at the cathode. On the other hand, the increase of the electrolyte concentration can reduce the ion transfer resistance, which can be proven by the slope shown in Fig. 7a. As a result, the performance increased with increasing the electrolyte concentration. Since the J_{sc} was increased with increasing the electrolyte concentration, the STH was increased with the electrolyte concentration, as shown in Fig. 7b. Similarly, the maximum power density also increased with increasing the electrolyte concentration. Accordingly, the FF increased with the electrolyte concentration.

Figure 8 shows the effect of the flow rate. In this measurement, the electrolyte concentration was kept at 0.2 M. The flow rate ranged from 100 μL min^{-1} to 1000 μL min^{-1}. As shown, the V_{oc} and J_{sc} were both reduced with increasing the flow rate in the

testing range. Although an increase in the flow rate can enhance the mass transport, more methanol could also reach the cathode, lowering the cathode performance. As a result, the V_{oc} decreased with increasing the flow rate. On the other hand, the increase of the flow rate means the decrease of the retention time. The retention time was shortened from 90.0 s to 9.0 s when the flow rate was increased from 100 μL min^{-1} to 1000 μL min^{-1}. The dramatic reduction of the retention time is not beneficial for methanol to be involved into the photoelectrochemical reactions at the photoanode. Therefore, the J_{sc} decreased with increasing the flow rate. Owing to the reduced J_{sc}, the STH, FF and maximum power density all decreased with the increase of the flow rate.

4. Conclusion

In this work, a micro membrane-less photoelectrochemical cell was developed for simultaneous production of hydrogen and electricity in the presence of methanol. The developed μML-PEC was consisted of a TiO_2 photoanode, a Pt/carbon paper electrode and a reaction microchamber. Experimental results showed that the hydrogen and electricity could be produced by this μML-PEC. Under given typical operating conditions, the STH was higher than the most reported data. The reason may be that the PEC miniaturization, and the elimination of the ion transport membrane, and the addition of the compact layer enhance the mass, electron and photon transfer, which eventually boosts the photoelectrochemical reaction rate. The effects of the light intensity, the methanol and electrolyte concentrations and the flow

rate on the performance were also studied. It was shown that the maximum power density increased with increasing the light intensity as a result of more photo-excited electron/hole pairs, while the FF and STH decreased. The decline of the FF is because the increments of the OCV and short circuit current density were more significant. The reduction of STH was due to the fact that increasing the light intensity also enhanced the electron/hole recombination rate. With respect to the methanol concentration, although its increase could result in the lowered cathode performance, the enhanced photoanode reaction was beneficial for the improvement in the performance. Therefore, the maximum power density, the STH and FF were all increased with increasing the methanol concentration. Once the methanol concentration was high enough, the positive effect resulting from the increased methanol concentration became ignorable. Regarding the electrolyte concentration, it was found that increasing the electrolyte concentration could improve the performance as a result of the enhanced photoelectrochemical and electrochemical reactions and lowered ionic transport resistance. Besides, it was also found that the performance of the μML-PEC decreased with increasing the flow rate because of the reduced retention time and more methanol oxidation at the cathode in the testing range. The obtained results fully demonstrated the feasibility of the developed μML-PEC. This work opens a new window for the design and optimization of the photoelectrochemical cell.

Acknowledgements

The authors gratefully acknowledge the financial supports of the National Natural Science Foundation of China (No.51325602, No.51576021 and No.51276208), the National High Technology Research and Development Program of China (863 Program) (No. 2015AA043503).

References

[1] K. Li, Y. Xu, Y. He, C. Yang, Y. Wang, J. Jia, Photocatalytic fuel cell (PFC) and dye self-photosensitization photocatalytic fuel cell (DSPFC) with BiOCl/Ti photoanode under UV and visible light irradiation, Energy & Environmental Science 47 (2013) 3490-3497.

[2] A. Fujishima, K. Honda, Electrochemical photolysis of water at a semiconductor electrode, Nature 238 (1972) 37–38.

[3] A. Mills, S.L. Hunte, An overview of semiconductor photocatalysis, Journal of Photochemistry & Photobiology A Chemistry 108 (1997) 1–35.

[4] A. Fujishima, X. Zhang, D.A. Tryk, Heterogeneous photocatalysis: from water photolysis to applications in environmental cleanup, International Journal of Hydrogen Energy 2007 (31) 2664–2672.

[5] J.M. Herrmann, Heterogeneous photocatalysis: fundamentals and applications to the removal of various types of aqueous pollutants, Catalysis Today 53 (1999) 115–129.

[6] D. Bahnemann, Photocatalytic water treatment: solar energy applications, Solar Energy 77 (2004) 445–459.

[7] J. Zhao, X.D. Yang, Photocatalytic oxidation for indoor air purification: a literature review, Building & Environment 38 (2003) 645–654.

[8] D.A. Tryk, A. Fujishima, K. Honda, Recent topics in photoelectrochemistry achievements and future prospects, Electrochimica Acta 45 (2000) 2363–2376.

[9] O. Khaselev, J.A. Turner, A monolithic photovoltaic–photoelectrochemical device

for hydrogen production via water splitting, Science 280 (1998) 425–427.

[10] M. Graetzel, Photoelectrochemical cells, Nature 414 (2001) 338–344.

[11] M.N. Chong, B. Jin, C.W.K. Chow, C. Saint, Recent developments in photocatalytic water treatment technology: A review, Water Research 44 (2010) 2997-3027.

[12] L. Li, R. Chen, X. Zhu, H. Wang, Y.Z. Wang, Q. Liao, D.Y. Wang, Optofluidic microreactors with TiO_2-coated fiber glass, ACS Applied Materials & Interfaces 5 (2013) 12548-12553.

[13] S. Malato, J. Blanco, C. Richter, B. Braun, M.I. Maldonado, Enhancement of the rate of solar photocatalytic mineralization of organic pollutants by inorganic oxidizing species. Applied Catalysis B: Environmental 17 (1998) 347-356.

[14] D.Y. Goswami, Recent Developments in photocatalytic detoxification and disinfection of water and air, ISES Solar World Congress 1999; Jerusalem, Israel, July. 1999.

[15] X. Cheng, R. Chen, X. Zhu, Q. Liao, X.F. He, S.Z. Li, L. Li, Optofluidic membrane microreactor for photocatalytic reduction of CO_2, International Journal of Hydrogen Energy 41 (4) (2016) 2457-2465.

[16] X. Cheng, R. Chen, X. Zhu, Q. Liao, L. An, D.D. Ye, X.F. He, S.Z. Li, L. Li, An optofluidic planar microreactor for photocatalytic reduction of CO_2 in alkaline environment, Energy 120 (2017) 276–282.

[17] R. Chen, X. Cheng, X. Zhu, Q. Liao, L. An, D.D. Ye, X.F. He, Z.B. Wang, High-performance optofluidic membrane microreactor with a mesoporous CdS/TiO_2

/SBA-15@carbon paper composite membrane for the CO_2, photoreduction, Chemical Engineering Journal 316 (2017) 911-918.

[18] L. Li, G.Y. Wang, R. Chen, X. Zhu, H. Wang, Q. Liao, Y.X. Yu, Optofluidics based micro-photocatalytic fuel cell for efficient wastewater treatment and electricity generation, Lab on a Chip 14 (2014) 3368-3375.

[19] L. Li, S. Xue, R. Chen, Q. Liao, X. Zhu, Z.B. Wang, X.F. He, H. Feng, X. Cheng, Performance characteristics of a membraneless solar responsive photocatalytic fuel cell with an air-breathing cathode under different fuels and electrolytes and air conditions, Electrochimica Acta 182 (2015) 280-288.

[20] L. Li, R. Chen, X. Zhu, Q. Liao, H. Wang, L. An, M. Zhang, A cascading gradient pore microstructured photoanode with enhanced photoelectrochemical and photocatalytic activities, Journal of Catalysis 344 (2016) 411-419.

[21] P. Lianos, Production of electricity and hydrogen by photocatalytic degradation of organic wastes in a photoelectrochemical cell: The concept of the Photo fuel cell: A review of a re-emerging research field, Journal of Hazardous Materials 185 (2011) 575-590.

[22] M. Antoniadou, V. Vaiano, D. Sannino, P. Lianos, Photocatalytic oxidation of ethanol using undoped and Ru-doped titania: Acetaldehyde, hydrogen or electricity generation, Chemical Engineering Journal 224 (2013) 144-148.

[23] M. Antoniadou, S. Sfaelou, P. Lianos, Quantum dot sensitized titania for photo-fuel-cell and for water splitting operation in the presence of sacrificial agents, Chemical Engineering Journal 254 (2014) 245-251.

[24] V.M. Daskalaki, M. Antoniadou, G.L. Puma, D.I. Kondarides, P. Lianos, Solar light-responsive Pt/CdS/TiO_2 photocatalysts for hydrogen production and simultaneous degradation of inorganic or organic sacrificial agents in wastewater, Environmental Science & Technology 44 (2010) 7200-7205.

[25] C. Zhang, M. Shao, F. Ning, S. Xu, Z. Li, M. Wei, D.G. Evans, X. Duan, Au nanoparticles sensitized ZnO nanorod@nanoplatelet core–shell arrays for enhanced photoelectrochemical water splitting, Nano Energy 12 (2015) 231-239.

[26] M. Antoniadou, P. Bouras, N. Strataki, P. Lianos, Hydrogen and electricity generation by photoelectrochemical decomposition of ethanol over nanocrystalline titania, International Journal of Hydrogen Energy 33 (2008) 5045-5051.

[27] M. Antoniadou, P. Lianos, Near Ultraviolet and visible light photoelectrochemical degradation of organic substances producing electricity and hydrogen, Journal of Photochemistry & Photobiology A Chemistry 204 (2009) 69-74.

[28] E.A. Hernández-Pagán, N.M. Vargasbarbosa, T.H. Wang, Y. Zhao, E.S. Smotkin, T.E. Mallouk, Resistance and polarization losses in aqueous buffer–membrane electrolytes for water-splitting photoelectrochemical cells, Energy & Environmental Science 5 (2012) 7582-7589.

[29] T. Tang, K. Li, D. Ying, T. Sun, Y. Wang, J. Jia, High efficient aqueous-film rotating disk photocatalytic fuel cell (RDPFC) with triple functions: Cogeneration of hydrogen and electricity with dye degradation, International Journal of Hydrogen Energy 39 (2014) 10258-10266.

[30] C. Yang, Y. He, K. Li, D. Ying, Y. Yao, T. Tang, Y. Wang, J. Jia, A highly efficient

dual rotating disks photocatalytic fuel cell with wedged surface TiO_2 nanopore anode and hemoglobin film cathode, Catalysts 6 (2016) 114.

[31] N. Balis, V. Dracopoulos, M. Antoniadou, P. Lianos, Solid-state dye-sensitized solar cells made of multilayer nanocrystalline titania and poly (3-hexylthiophene), Journal of Photochemistry & Photobiology A Chemistry 214 (2010) 69–73.

[32] Á.A. Ramírezsantos, P. Acevedopeña, E.M. Córdoba, Photo-assisted electrochemical copper removal from cyanide solutions using porous TiO_2 thin film photo-anodes, Materials Research 17 (2012) 69-77.

[33] B. Seger, G.Q. Lu, L. Wang, Electrical power and hydrogen production from a photo-fuel cell using formic acid and other single-carbon organics, Journal of Materials Chemistry 22 (2012) 10709-10715.

[34] T.L. Villarreal, R. Gomez, M. Neumann-Spallart, N. Alonso-Vante, P. Salvador, Semiconductor photooxidation of pollutants dissolved in water: A kinetic model for distinguishing between direct and indirect interfacial hole transfer. I. Photoelectrochemical experiments with polycrystalline anatase electrodes under current doubling and absence of recombination, The Journal of Physical Chemistry B 108 (2004) 15172-15181.

[35] I. Mora-Sero, T.L. Villarreal, J. Bisquert, A. Pitarch, R. Gomez, P. Salvador, Photoelectrochemical behavior of nanostructured TiO_2 thin-film electrodes in contact with aqueous electrolytes containing dissolved pollutants: A model for distinguishing between direct and indirect interfacial hole transfer from photocurrent measurement, The Journal of Physical Chemistry B 109 (2005) 3371-3380.

[36] M.F.J. Dijkstra, H.J. Panneman, J.G.M. Winkelman, J.J. Kelly, A.A.C.M. Beenackers, Modeling the photocatalytic degradation of formic acid in a reactor with immobilized catalyst, Chemical Engineering Science 57 (2002) 4895-4907.

[37] B. Seger, P.V. Kamat, Fuel cell geared in reverse: photocatalytic hydrogen production using a TiO_2/Nafion/Pt membrane assembly with no applied bias, The Journal of Physical Chemistry C 113 (2009) 18946-18952.

[38] T. Bak, J. Nowotny, M. Rekas, C.C. Sorrell, Photo-electrochemical hydrogen generation from water using solar energy. Materials-related aspects, International Journal of Hydrogen Energy 27 (2002) 991–1022.

[39] J.W.A. Iii, M.R. Shaner, K.A. Walczak, I.D. Sharp, S. Ardo, Experimental demonstrations of spontaneous, solar-driven photoelectrochemical water splitting, Energy & Environmental Science 8 (2015) 2811-2824.

[40] M. Ebaid, J.H. Kang, S.H. Lim, J.S. Ha, J.K. Lee, Y.H. Cho, S.W. Ryu, Enhanced solar hydrogen generation of high density, high aspect ratio, coaxial InGaN/GaN multi-quantum well nanowires, Nano Energy 12 (2015) 215-223.

[41] X.J. Shi, H. Jeong, S.J. Oh, M. Ma, K. Zhang, J. Kwon, I.T. Choi, I.Y. Choi, H.K. Kim, J.K. Kim, J. H. Park, Unassisted photoelectrochemical water splitting exceeding 7% solar-to-hydrogen conversion efficiency using photon recycling, Nature Communications 7 (2015) 11943.

[42] J. Juodkazytė, G. Seniutinas, B. Šebeka, I. Savickaja, T. Malinauskas, K. Badokas, K. Juodkazis, S. Juodkazis, Solar water splitting: Efficiency discussion, International Journal of Hydrogen Energy 41 (2016) 11941-11948.

[43] M. Antoniadou, D.I. Kondarides, D. Labou, S. Neophytides, P. Lianos, An efficient photoelectrochemical cell functioning in the presence of organic wastes, Solar Energy Materials & Solar Cells 94 (2010) 592-597.

Table list

Table 1 STH comparison between the present study and previous studies.

Table 1 STH comparison between the present study and previous studies

Type of cell	Light source	Catalyst	Electrolyte Anode/Cathode	Reactant	STH	Ref.
Two compartments	Xe lamp	TiO_2	0.5 M NaOH/ 0.5 M NaOH	5% v. ethanol	0.016	23
H-shaped	360 nm UV light	TiO_2	1.0 M NaOH / 1.0 M H_2SO_4	Water 20% v. ethanol	0.031 0.199	26
Rotating disk	254 nm UV light	TiO_2	2 .0 M NaOH / 1.0 M H_2SO_4	Water Reactive brilliant red X-3B	0.077 0.119	29
Single compartment with Nafion–Pt/C cathode	350 nm UV light	TiO_2	0.2 M NaOH	Water 20% v. ethanol	0.101 0.224	43
Membrane electrode assembly	Xe lamp	TiO_2	1 M formic acid / 0.1 M H_2SO_4	Formic acid	0.002	33
μML-PEC	370 nm UV light	TiO_2	0.2 M KOH	0.5 M methanol	0.305	Ours

Figure captions

Figure 1 (a) Schematic of the μML-PEC, (b) Image of the fabricated μML-PEC.

Figure 2 (a) The XRD pattern of the TiO_2 film on FTO conducting glass; (b) The top-view SEM image of the TiO_2 film; (c) The side-view SEM image of the TiO_2 film; (d) The side-view SEM image of the compact layer.

Figure 3 Photo-response of the μML-PEC: (a) Photo-voltage response, (b) Photo-current response. Light intensity: 5 mW cm^{-2}; methanol concentration: 0.5 M; KOH concentration: 0.2 M; flow rate: 100 μL min^{-1}.

Figure 4 (a) Typical polarization curve and (b) long-term discharging performance of the μML-PEC. Light intensity: 5 mW cm^{-2}; methanol concentration: 0.5 M; KOH concentration: 0.2 M; flow rate: 100 μL min^{-1}.

Figure 5 Effect of the light intensity: (a) variation of the polarization curve, (b) variations of the maximum power density, FF and STH. Methanol concentration: 0.5 M; KOH concentration: 0.2 M; flow rate: 100 μL min^{-1}.

Figure 6 Effect of the methanol concentration: (a) variation of the polarization curve, (b) variations of the maximum power density, FF and STH. Light intensity: 5 mW cm^{-2}; KOH concentration: 0.2 M; flow rate: 100 μL min^{-1}.

Figure 7 Effect of the electrolyte concentration: (a) variation of the polarization curve, (b) variations of the maximum power density, FF and STH. Light intensity: 5 mW cm^{-2}; methanol concentration: 0.5 M; flow rate: 100 μL min^{-1}.

Figure 8 Effect of the flow rate: (a) variation of the polarization curve, (b) variations of the maximum power density, FF and STH. Light intensity: 5 mW cm^{-2}; methanol concentration: 0.5 M; KOH concentration: 0.2 M.

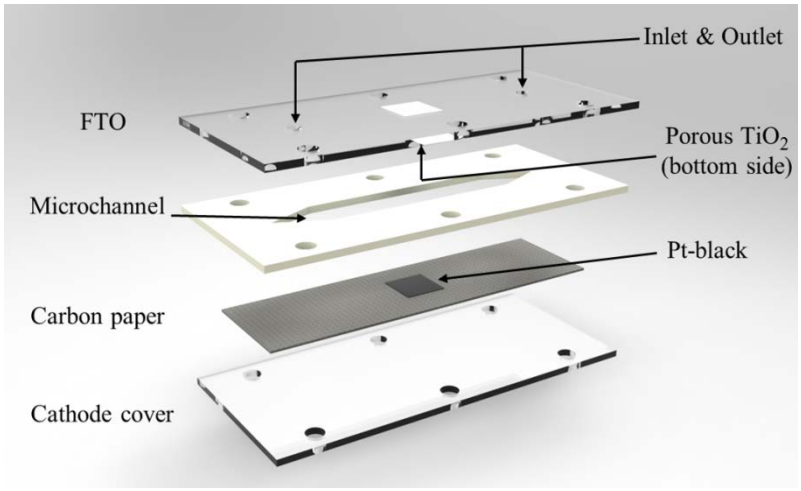

(a)

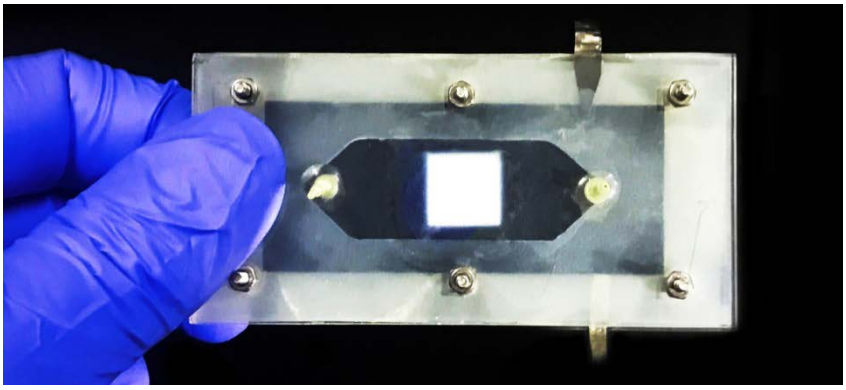

(b)

Fig. 1 (a) Schematic of the μML-PEC, (b) Image of the fabricated μML-PEC.

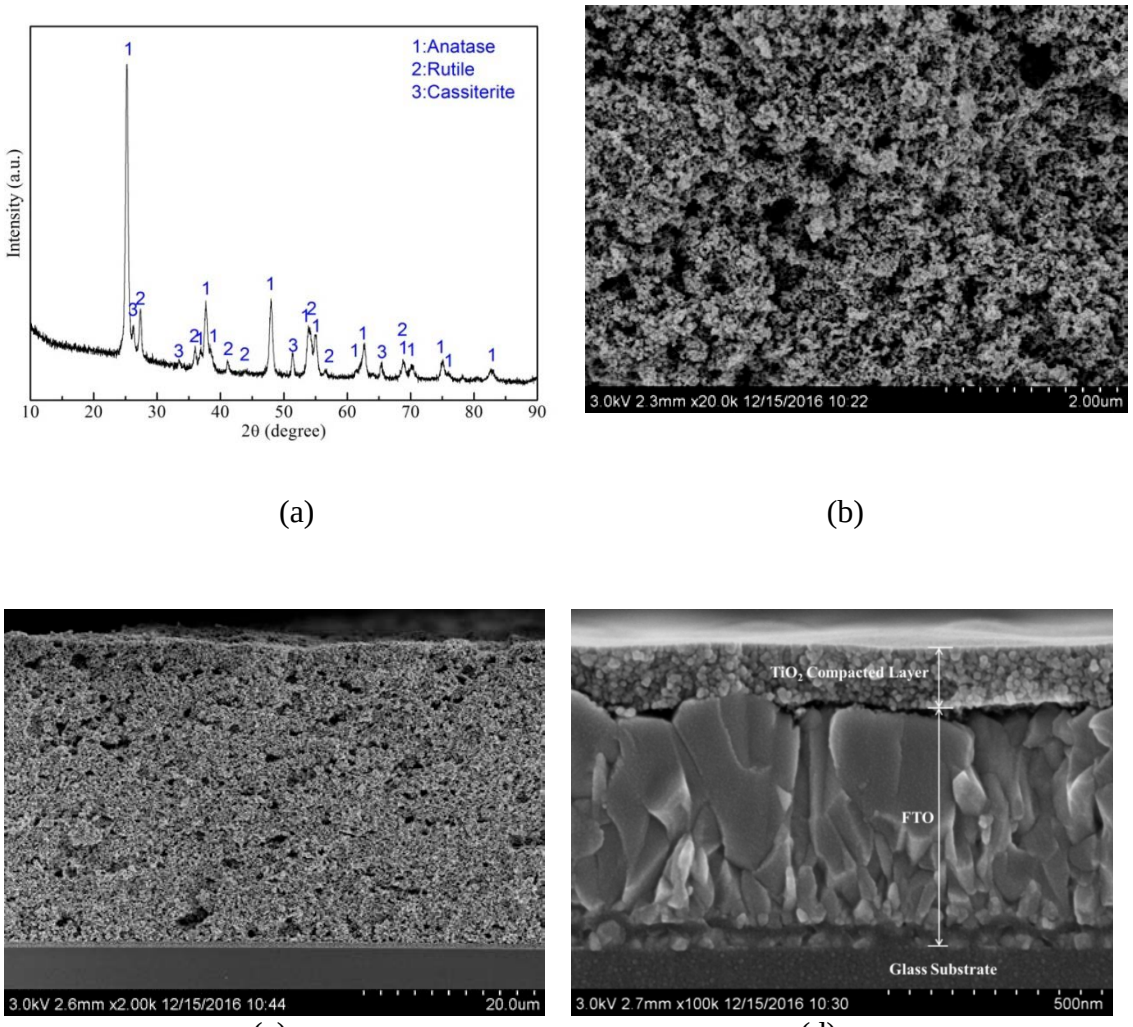

Fig. 2 (a) The XRD pattern of the TiO_2 film on FTO conducting glass; (b) The top-view SEM image of the TiO_2 film; (c) The side-view SEM image of the TiO_2 film; (d) The side-view SEM image of the compact layer.

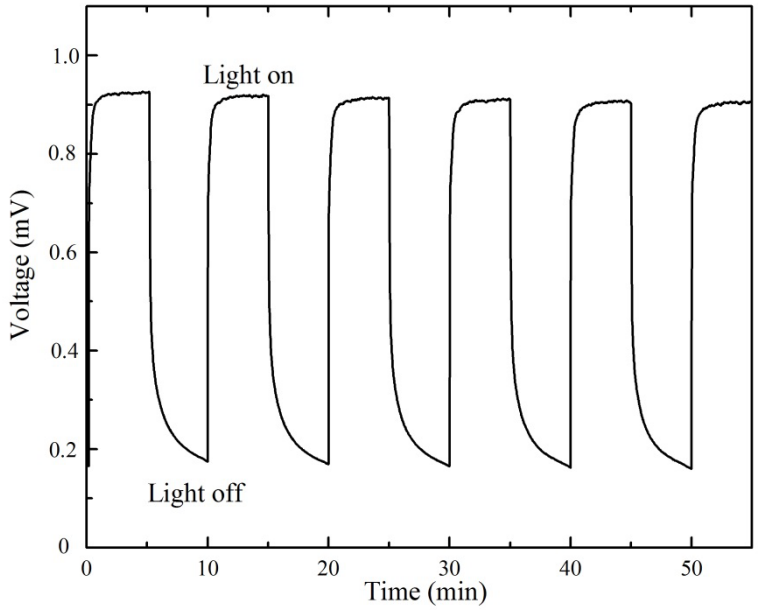

(a)

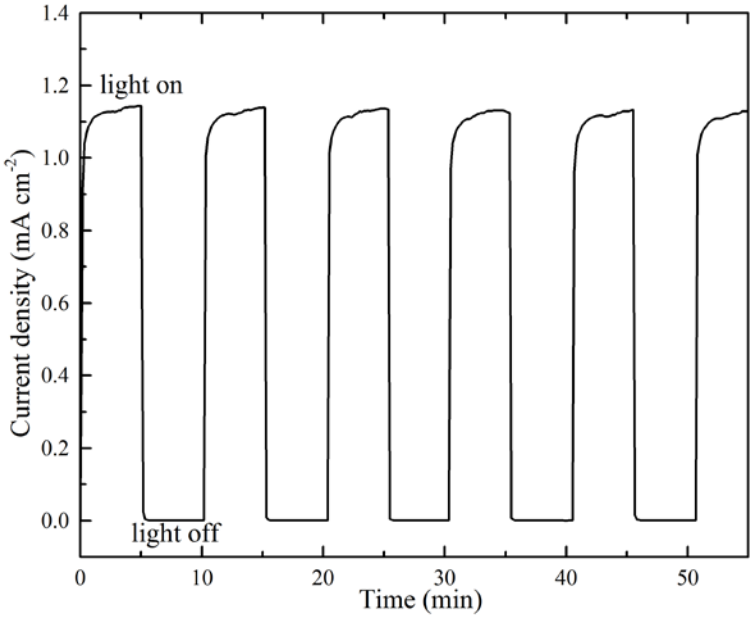

(b)

Fig. 3 Photo-response of the μML-PEC: (a) Photo-voltage response, (b) Photo-current response. Light intensity: 5 mW cm^{-2}; methanol concentration: 0.5 M; KOH concentration: 0.2 M; flow rate: 100 μL min^{-1}.

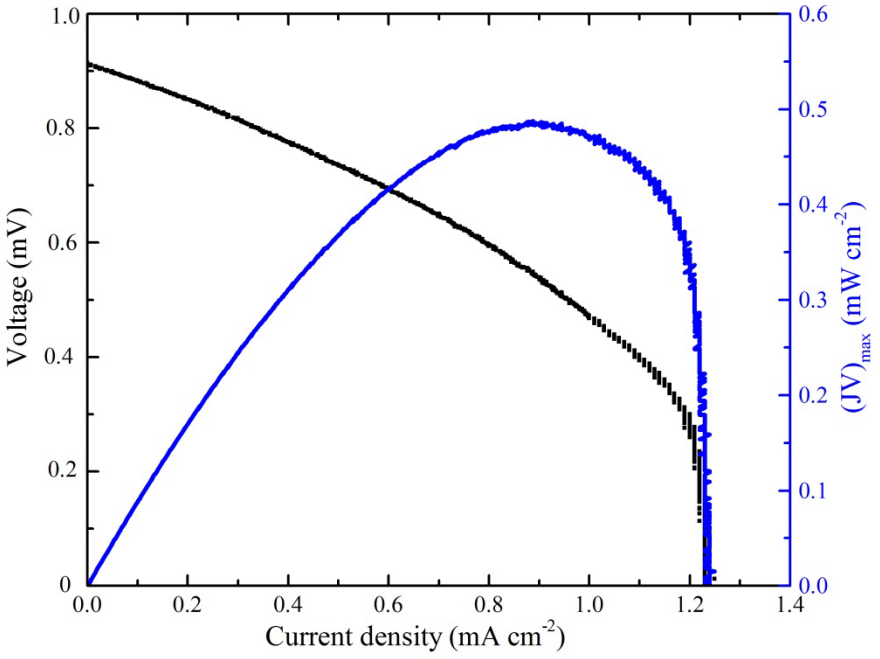

(a)

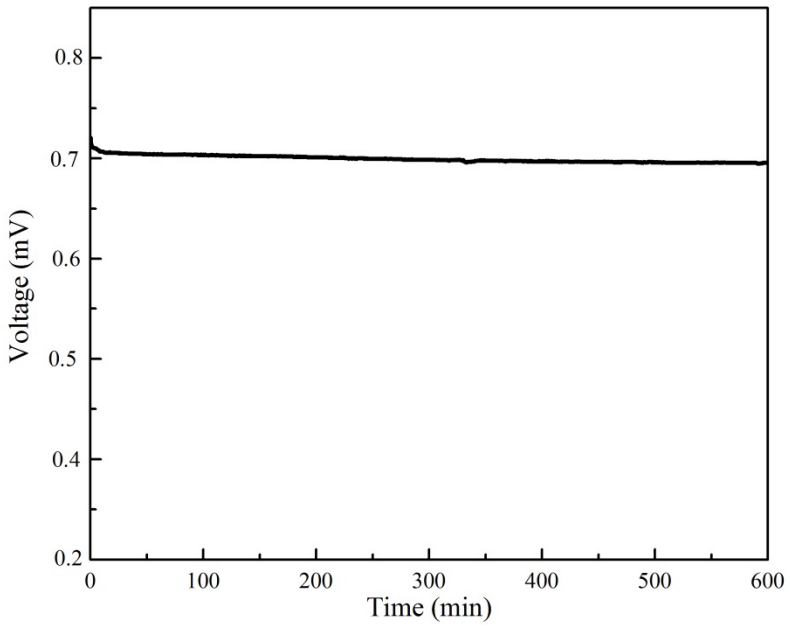

(b)

Fig. 4 (a) Typical polarization curve and (b) long-term discharging performance of the μML-PEC. Light intensity: 5 mW cm^{-2}; methanol concentration: 0.5 M; KOH concentration: 0.2 M; flow rate: 100 μL min^{-1}.

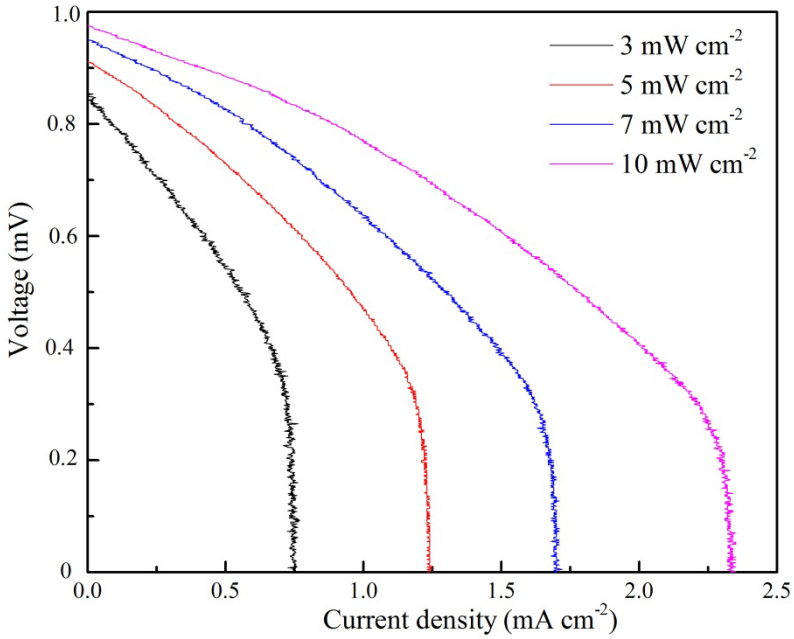

(a)

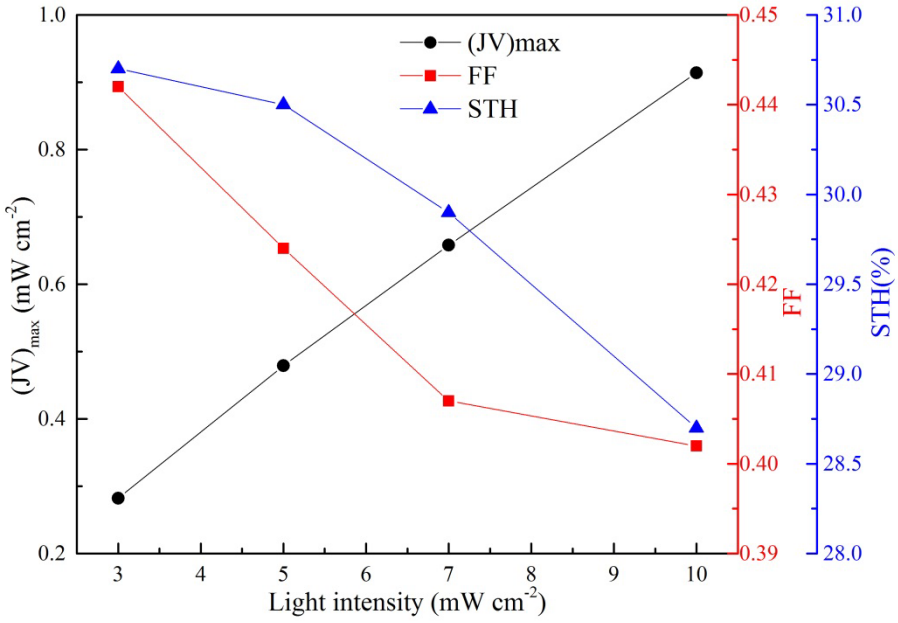

(b)

Fig. 5 Effect of the light intensity: (a) variation of the polarization curve, (b) variations of the maximum power density, FF and STH. Methanol concentration: 0.5 M; KOH concentration: 0.2 M; flow rate: 100 μL min^{-1}.

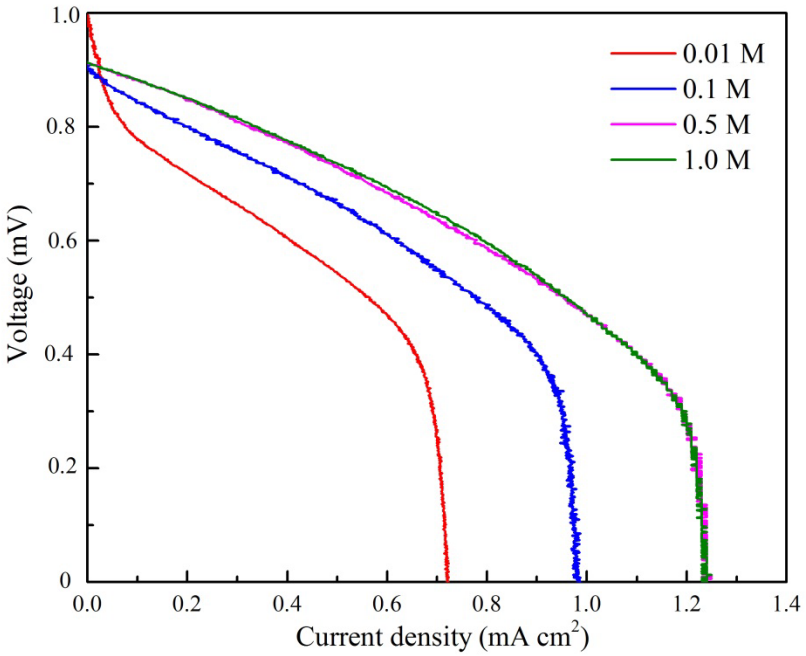

(a)

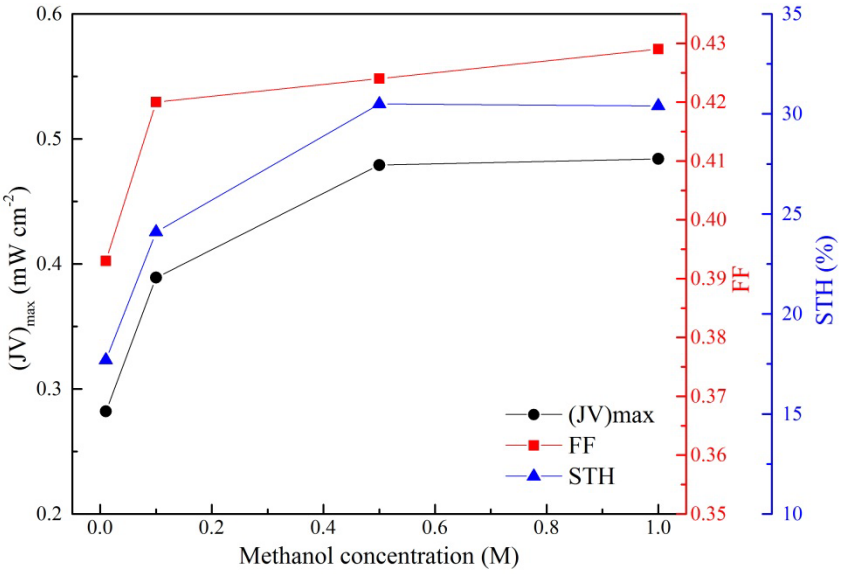

(b)

Fig. 6 Effect of the methanol concentration: (a) variation of the polarization curve, (b) variations of the maximum power density, FF and STH. Light intensity: 5 mW cm^{-2}; KOH concentration: 0.2 M; flow rate: 100 μL min^{-1}.

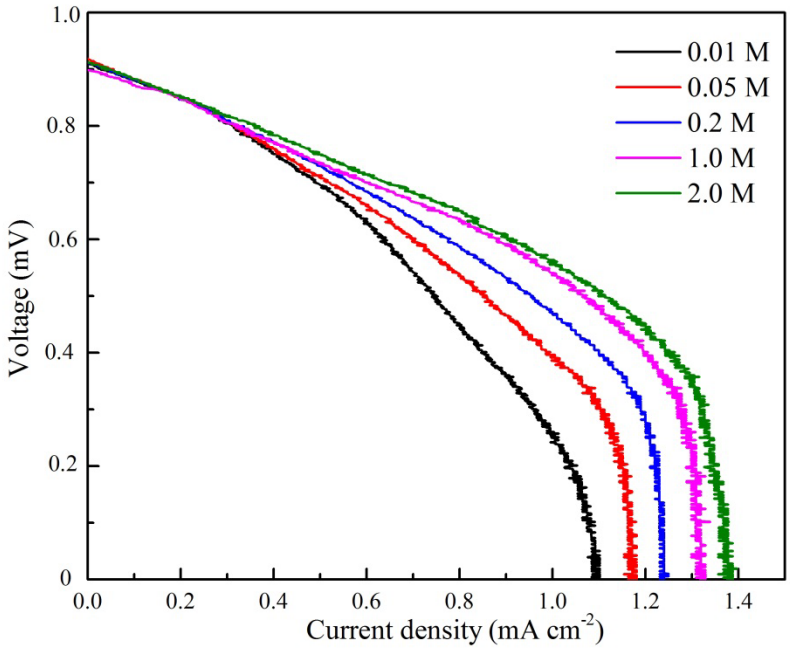

(a)

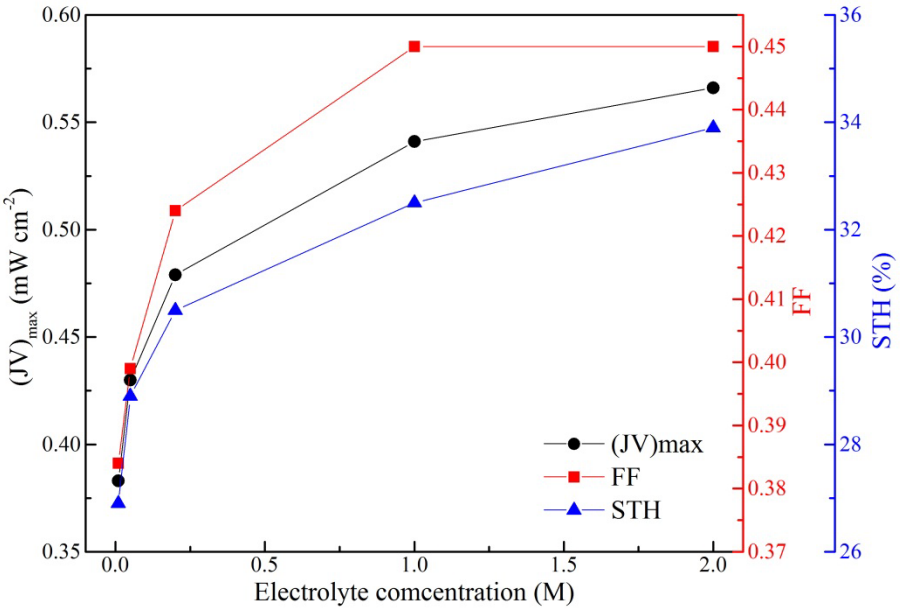

(b)

Fig. 7 Effect of the electrolyte concentration: (a) variation of the polarization curve, (b) variations of the maximum power density, FF and STH. Light intensity: 5 mW cm^{-2}; methanol concentration: 0.5 M; flow rate: 100 μL min^{-1}.

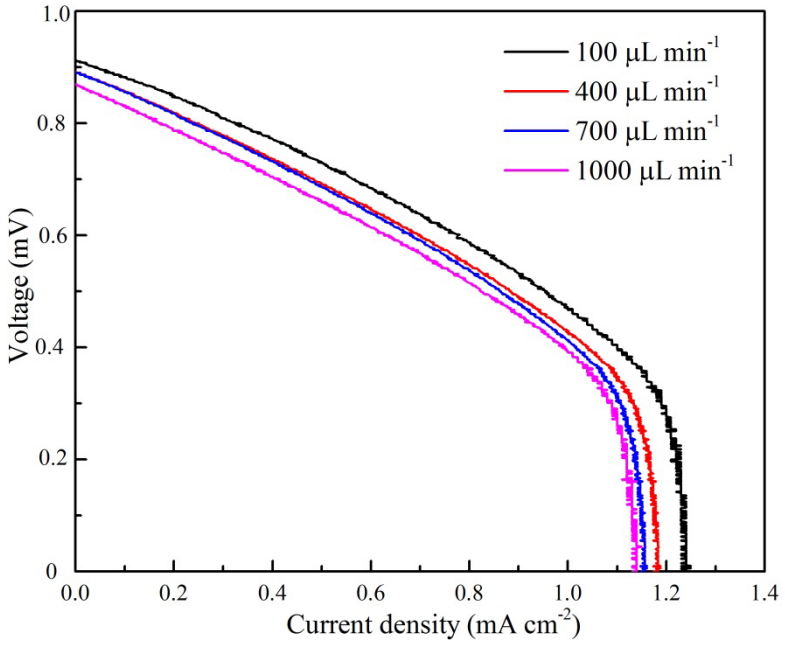

(a)

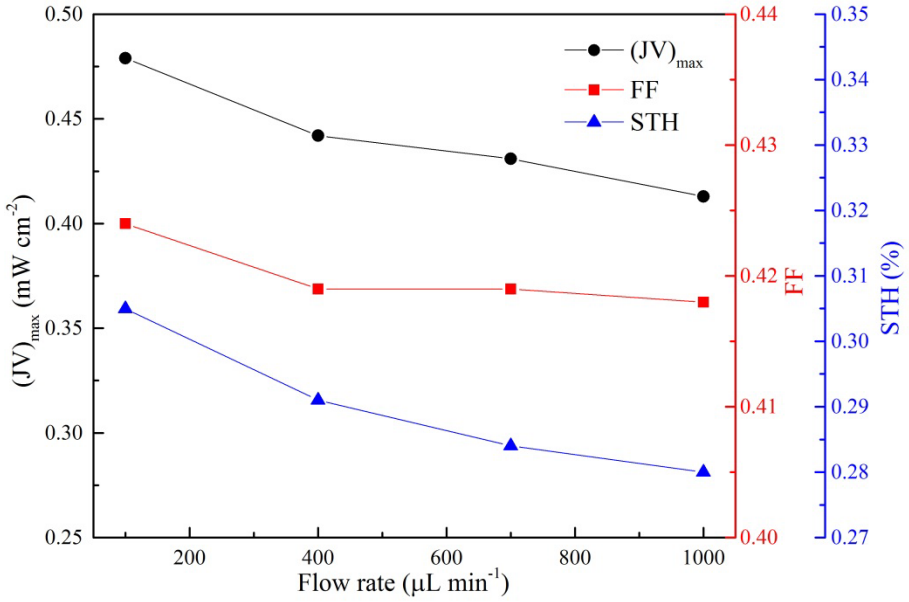

(b)

Fig. 8 Effect of the flow rate: (a) variation of the polarization curve, (b) variations of the maximum power density, FF and STH. Light intensity: 5 mW cm^{-2}; methanol concentration: 0.5 M; KOH concentration: 0.2 M.